Engineering Structures 222 (2020) 111002

Contents lists available at ScienceDirect

Engineering Structures

journal homepage: www.elsevier.com/locate/engstruct

# Accounting for spectral shape in a simplified method of analyzing friction pendulum systems

Tianye Yang*, Nasser A. Marafi, Paolo M. Calvi, Richard Wiebe, Marc O. Eberhard, Jeffrey W. Berman

*Department of Civil and Environmental Engineering, University of Washington, USA*

ARTICLE INFO

*Keywords:*
Seismic isolation
Simplified analysis
Displacement spectrum
Friction pendulum system

ABSTRACT

This paper examines the effect of subduction zone and basin amplified motions on the accuracy of using a simplified method to analyze Friction Pendulum Systems, which is the basis for many international code provisions. This method estimates the maximum displacement demand for Friction Pendulum System isolated structures from analyzing a single degree of freedom system with equivalent period and damping coefficient. Friction Pendulum Systems with equivalent natural period between 1.5 s and 5 s and equivalent damping ratio from 16% to 32% were considered when subjected to over 400 motions. The considered ground motions include crustal and subduction zone motions, with and without basin amplification effect. Ratios of analysis-to-design maximum displacements corresponding to each ground motion are computed. A displacement-spectrum shape correction factor is proposed to improve the accuracy of the simplified method. This correction factor takes into account the irregularity of the 5% damped displacement spectrum that depends on the equivalent period and damping ratio at design displacement of the isolation system.

## 1. Introduction

Simplified methods of analyzing an equivalent single-degree-of-freedom system are often adopted in modern building codes for analyzing Friction Pendulum Systems (FPSs) for seismic isolation (e.g. ASCE [1] and Eurocode 8 [2]). These simplified methods also provide a lower bound for the force values that should be used in place of values obtained from dynamic time-history analysis [1]. Thus the accuracy of such methods is of great importance.

These simplified methods analyze base-isolated systems by representing them with single degree of freedom systems that have equivalent linear elastic and viscous damping properties. These methods can be applied to the design of not only FPSs, but also other systems with well-characterized hysteretic behavior. The accuracy of such methods has been studied by numerous researchers [3–7]. These studies have shown that the simplified methods are able to reasonably predict the mean maximum displacement calculated from nonlinear time history analyses for a suite of ground motions, however, there is often large standard deviations [5]. Moreover, these studies have largely considered strong ground motion recordings from crustal earthquakes recorded on stiff-soil site or medium-soil site conditions. To further explore the accuracy and limitations of simplified methods, work in [8] considered near-field and soft-soil ground motions. Nonetheless, the accuracy of these methods has never been assessed considering ground motions generated from subduction zones or amplified by basin effects, which modify the characteristics of response spectra [9–11].

The simplified method evaluated herein is the effective stiffness and damping method that is described in design code provisions for base-isolated structures (e.g. ASCE [1] and Eurocode 8 [2]). To shed light on the accuracy of using this method for FPS with subduction zone motions or motions amplified due to basin effects, this paper presents:

- Information on four sets of ground motions considered in this study, which include both crustal and subduction zone ground motions, with and without basin effects.
- A comparison between the average values of displacement reduction factors, as defined in Section 2, obtained through analyses with considered ground motion datasets and the values calculated based on empirical equations provided by different code provisions.
- Results of maximum absolute displacement from nonlinear time history analysis in comparison to design displacement computed from the simplified method.
- A newly proposed displacement-spectrum shape correction factor

* Corresponding author.
*E-mail address:* tianyy3@uw.edu (T. Yang).

https://doi.org/10.1016/j.engstruct.2020.111002
Received 27 February 2020; Received in revised form 13 May 2020; Accepted 23 June 2020

that improves the accuracy of the simplified method for FPS, by taking into account the "irregularity" of the seismic input (expressed in the form of an elastic displacement spectrum). This correction factor depends on the effective period and effective damping ratio of the isolation system at design displacement.

## 2. Overview of current design procedures

With minor differences between them, the simplified methods adopted in modern design code provisions (e.g. [1,2]) for base-isolated structures are based on displacement-based design principles. The simplified method involves the following steps: (a) select the design displacement of the structure, (b) construct the hysteretic loop of the isolator at the design displacement level, (c) estimate the equivalent SDOF system's effective stiffness and effective damping ratio, (d) calculate a displacement reduction factor based on effective damping ratio, (e) obtain the seismic input in the form of displacement response spectrum at 5% damping ratio, (f) apply displacement reduction factor to the 5% damped displacement response spectrum to obtain reduced displacement spectrum corresponding to the effective damping ratio of the isolation system, (g) estimate the effective period of vibration of the system, (h) obtain displacement demand from the reduced displacement spectrum given the effective period of vibration, and (i) repeat steps (b) to (h) until the difference between design displacement and displacement demand is sufficiently close. With a converged design displacement value, the base shear demand can be calculated from the hysteretic loop of the isolation system and is then distributed over the height of the superstructure.

The main difference between the different code provisions is in the way the displacement reduction factor is calculated. The displacement reduction factor (i.e., damping reduction factor) is defined as the spectral displacement ratios at different damping levels normalized to the 5% damped displacement spectrum. As a function of the equivalent damping ratio of the isolation system at the design displacement, displacement reduction factors aim to account for the effect of hysteretic damping on the force and displacement response of the building.

Fig. 1 shows a comparison from various building codes between the displacement reduction factors, $\eta$, versus the damping ratio, $\zeta$, for ASCE 7-16 [1], and Eurocode 8 (1994) [12] and (2004) [2]. It should be noted that ASCE 7-16 provides a table of damping reduction factors given several damping ratios (other values are linearly extrapolated), while Eurocode 8 (1994) and (2004) use equations of $\sqrt{7/(2+\zeta)}$ and $\sqrt{10/(5+\zeta)}$, respectively. These three cases were chosen here because the Eurocode 8 (1994) equation is recommended for Direct Displacement Based Design method [13], the other two are the current design provisions in the United States and Europe, respectively. A more thorough review can be found in [14]. Compared to the other codes the Eurocode 8 (1994) provides the most unconservative results (i.e. greater reduction factor given a damping ratio), and the ASCE 7-16 provides the most conservative one.

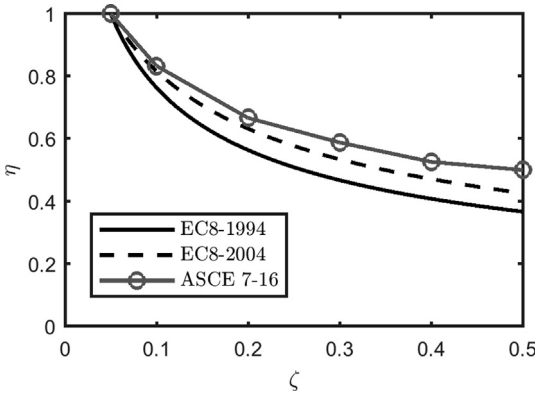


**Fig. 1.** A Comparison of the displacement reduction factor with respect to damping ratio for Eurocode 8 (1994)[12], Eurocode 8 (2004) [2], and ASCE 7-16 [1].

While these equations provide different levels of displacement reduction for a given damping ratio, they are all period independent. Numerous researchers have studied the accuracy of these equations [14–16]. Lin and Chang [14] focused on the application of damping reduction factors on the acceleration spectrum, velocity spectrum, and displacement spectrum, while Bommer and Mendis [15] and Lin and Chang [16] investigated the accuracy of these equations for varying site classes, earthquake magnitude, site-to-source distances, and duration. Near source directivity effects were also considered by Bommer and Mendis [15], however, subduction zone earthquakes or basin amplified ground motions were not included in any of these previous studies.

## 3. Evaluation of current simplified method under ground motions with different characteristics

### 3.1. Description of the ground motion datasets used

To evaluate the accuracy of the simplified method on FPS with subduction zone motions and basin amplified motions, four sets of ground motions were considered:

- 60 ground motions were selected from the NGA-WEST2 database [17] and scaled to match the $MCE_R$ design spectrum for Seattle (Site Class C) based on NEHRP 2015 [18]. First, all ground motions from NGA-WEST2 were screened based on the following criteria: (1) an unscaled peak ground acceleration of at least 0.05 g, (2) a source-to-site (Joyner-Boore) distance between 5 and 100 km, (3) no pulse-like characteristics. Then, to select the ground motions providing the best spectral match, each ground motion in the database was scaled to have a minimum square-root-the-sum-of-squares of the log error compared to the design spectrum for a period range of 1–6 s. This period range was chosen because it was deemed appropriate for typical equivalent periods of FPS-isolated structures. Finally, 60 ground motions with the least square-root-the-sum-of-squares of the log errors were selected with scale factors limited between 0.2 and 5. This set of ground motions is a benchmark for the study given that it represents strong crustal earthquakes as studied by previous researchers [3–7]. A comparison between the design spectrum and the average scaled spectrum is shown in Fig. 2(a). The median 5–95% significant duration was approximately 26 s with a coefficient of variation of 130%. This set of motions is denoted as "Crustal" in the following discussion.
- Based on geological evidence, the Cascadia Subduction Zone (CSZ) is capable of generating megathrust earthquakes up to magnitude-9 (M9) that may severely affect the Pacific Northwest in the United States [19,20]. In addition, many cities in the Pacific Northwest (e.g. Seattle) are underlain by a deep sedimentary basin [21] that is known to amplify ground-shaking intensity [11]. Ideally, measured ground motions generated by CSZ with basin effects should be used. However, they do not currently exist. Due to the paucity of recordings, Frankel et al. [22] used physics-based simulations to generate ground-motions for 30 scenarios of an M9 earthquake in the Pacific Northwest. This paper uses ground-motions produced from these simulations for Seattle where the displacement spectrum of these simulated motions are shown in Fig. 2(b). More recently, Marafi et al. [11] showed that deep basins modify subduction zone ground motions differently than has been observed for crustal motions, and that the Seattle basin, which is particularly deep, results in significant amplification of long period ground motion. Thus it is valuable to evaluate how these characteristics may affect the accuracy of the simplified method for FPS. This set of motions is denoted as "M9" in the following discussion.
- The last two sets of motions were developed by Chandramohan et al.

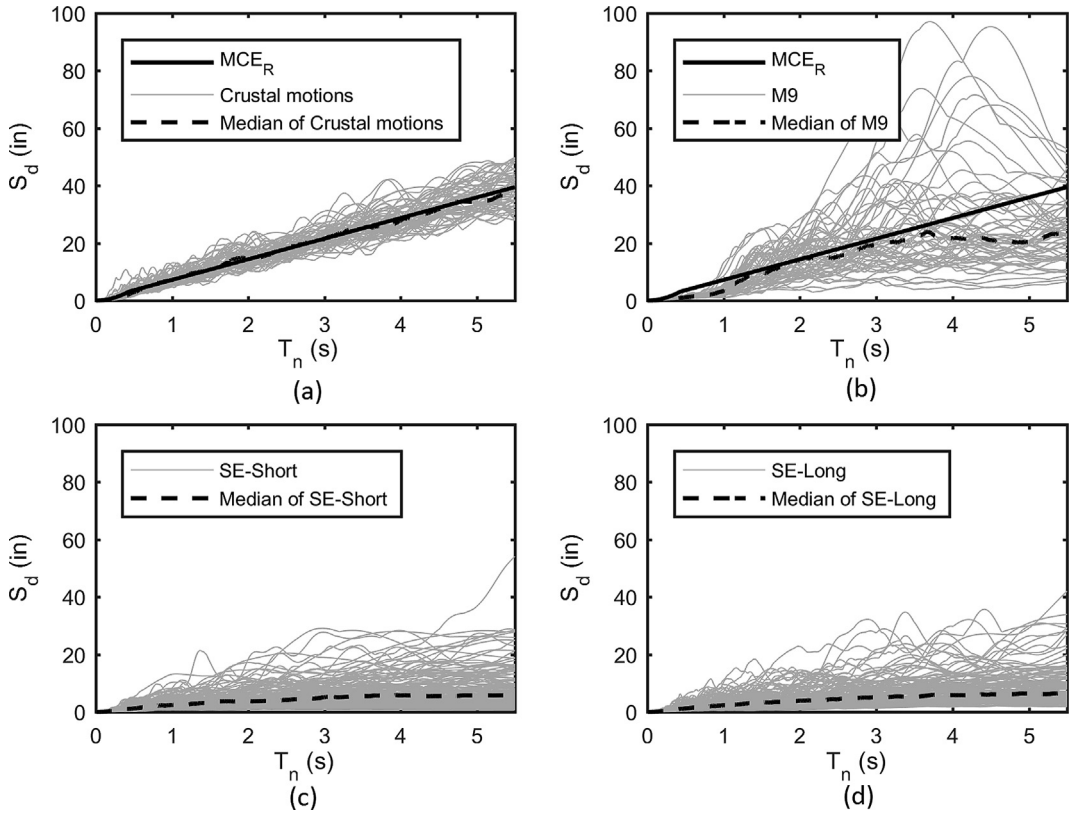


**Fig. 2.** Spectral displacement with respect to period for (a) NGA-West-2 motions scaled to the $MCE_R$ design spectrum from NEHRP, (b) simulated magnitude-9 CSZ earthquake in Seattle, (c) and (d) spectrally equivalent motions with short and long significant durations, respectively, developed by Chandramohan et al. [23].

[23]. Each of these two sets have 73 ground-motion pairs (X and Y component) and were aimed at evaluating the influence of ground motion duration on structural collapse capacity. One set of ground motions was chosen from subduction zone earthquakes and the other from crustal earthquakes. Each individual record in the Crustal motion dataset was chosen to have a spectrally equivalent record in the subduction zone motion dataset, thus the primary difference between the two sets is the significant duration of the motion. These two sets of motions are denoted as “SE - Long” and “SE - Short” respectively in the following discussion.

### 3.2. Numerical analysis procedure

To evaluate the accuracy of using the simplified method to analyze FPS when subjected to ground motions with different characteristics, single-degree-of-freedom systems that characterize the hysteretic behavior of FPS were designed and analyzed. A design was completed for each ground motion individually using the simplified method described above and for a range of FPS properties (period and damping) as described below. Then, nonlinear response history analysis was performed in OpenSees [24] for each designed FPS and ground motion, in which the FPS was modeled using the Single Friction Pendulum Bearing Element [25]. The resulting maximum displacements were recorded to compare with the displacement predicted using the simplified method.

The equivalent lateral force procedure, ASCE 7-16 [1] requires that “the effective period of the isolated structure is greater than three times the elastic, fixed-base period of the structure above the isolation system” and “the effective period of the isolated structure at the maximum displacement is less than or equal to 5.0 s”. Thus for each ground motion considered, FPS with equivalent natural periods from 1.5 to 5.0 s (with an increment of 0.5 s) were considered in this study.

For the design of FPS, the method described in Calvi et al.[26] was followed. This method follows the direct displacement-based design method proposed by Priestley et al. [13]. The only difference between this method and the one described in Section 2 is that the procedure becomes non-iterative by introducing a parameter $\alpha$ (which is equal to the ratio between the designed base shear and force required to activate the slider). By selecting an $\alpha$ value, the effective damping ratio can be calculated using Eq. 1:

$$\zeta = 2/\alpha\pi \tag{1}$$

The displacement reduction factor can then be calculated using the equations or tables that generated the curves in Fig. 1, depending on the code provisions used. In this study, all three cases presented in Fig. 1 were considered. Finally, the design displacement can be obtained either from a predetermined effective period (or vice versa) using reduced displacement spectrum.

An $\alpha$ range of 2–4 (with an increment of 0.5) was chosen for this study to represent FPSs with different effective damping ratios. These are realistic $\alpha$ values based on Calvi and Calvi [27]. In addition, this range of $\alpha$ is equivalent to an effective damping ratio range from 16% to 32%. The upper bound of the damping ratio was set to be approximately equal to 30%, which was selected because it is the limit for using the equivalent lateral force procedure in ASCE 7-16 [1].

### 3.3. Numerical results

For brevity, only detailed results associated with using the displacement reduction equation provided by Eurocode 8 (1994) [12] are presented in this section. While only the final outcome is reported for the other two cases, detailed results can be found in Yang [28].

Fig. 3 shows the boxplots of the analysis-to-design ratios for all analyses with respect to the equivalent natural period of the isolation systems ($T_n$) for the four ground-motion sets previously described. For each $T_n$ the extent of the box represents the 25*th* and 75*th* percentile, the horizontal line within the box represents the 50*th* percentile, and the

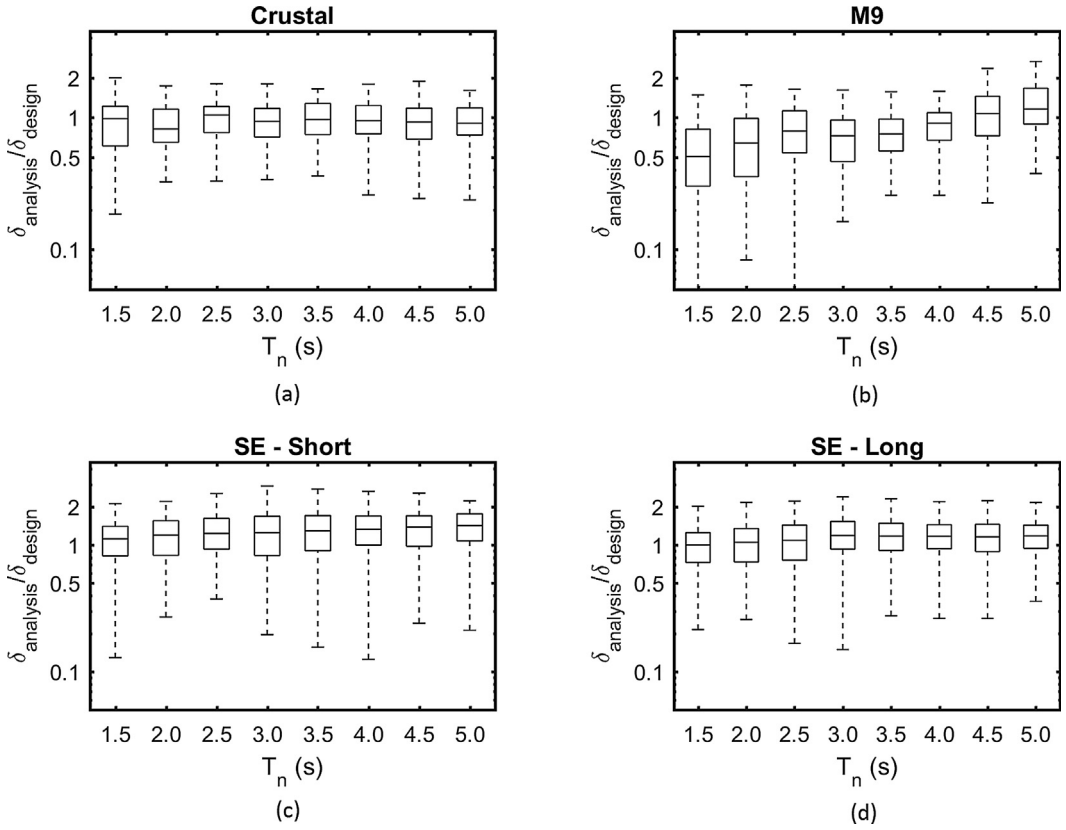


**Fig. 3.** Numerical results (for $\alpha$ equals to 3) of the ratio (in log-scale) between maximum absolute displacement from NLTHA and design displacement varying by design period for each ground motion dataset.

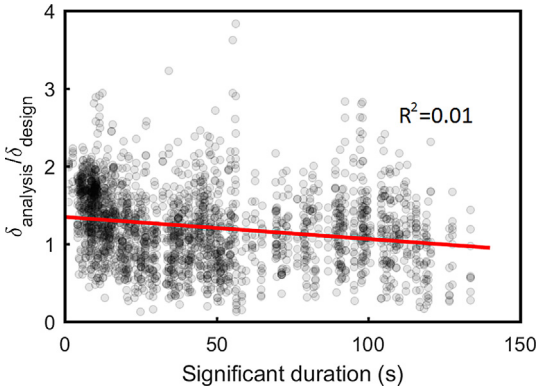


**Fig. 4.** Design-to-analysis ratio with respect to (5–95%) significant duration including results from SE-Short and SE-Long ground-motion sets.

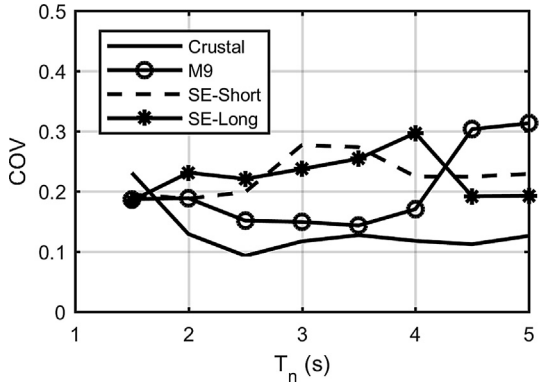


**Fig. 5.** Numerical results (for $\alpha$ equals to 3) of the coefficient of variance (COV) of the analysis-to-design ratio versus design period for each ground motions dataset.

extent of the whiskers corresponds to the minimum and maximum observed values. For brevity, only the results pertaining to $\alpha$ equals to 3 are presented here. Similar trends were observed for all the other $\alpha$ values considered [28].

Fig. 3a shows that the analysis-to-design ratios considering the Crustal ground motion set have median values that are approximately equal to 1.0 (ranging from 0.82 to 1.04) at all period values. However, within each period there is variability in analysis-to-design ratios. This variability can be quantified using the coefficient of variation of the analysis-to-design ratios (plotted in Fig. 5a) which ranges from 0.09 to 0.23 for the Crustal ground-motion set. This large variability indicates that even when the median ratio is approximately 1.0, the general prediction is not sufficiently accurate. Thus, the simplified method works well in an average sense, however, when considering all individual analyses, the accuracy of the method could be improved.

Fig. 3b shows that the analysis-to-design ratios using the M9 ground-motion set have median values mostly smaller than 1.0 (ranging from 0.51 to 1.16). An analysis-to-design ratio less than 1.0 means that the design is conservative. It is worth mentioning that the applied simplified method incorporated the most unconservative damping reduction equation, when other existing equations were used (e.g., Eurocode 8 (2004)[2] or ASCE 7-16 [1]), the final results were more conservative [28]. However, these differences would not account for the apparent period dependency in the analysis-to-design ratio (Fig. 3b). For example, 1.5-s oscillators had a median analysis-to-design ratio of 0.51 whereas this ratio was around 1.16 for oscillator periods around 5.0 s. This period dependence is likely due to ground-motion characteristics [29] not currently accounted for in the displacement reduction factor estimate. The coefficient of variation of the analysis-to-

design ratios (plotted in Fig. 5b) ranges from 0.14 to 0.31, which is greater than those from the Crustal set.

For the SE - Short and SE - Long datasets, similar results were observed in terms of accuracy. Fig. 4 shows the analysis-to-design ratio with respect to (5–95%) significant duration. The least squares linear regression line is also shown in the plot. An R squared value of 0.01 means that significant duration does not affect the accuracy of the simplified method. In general, for this study, the median analysis-to-design ratios are slightly above 1.0, ranging from 1.1 to 1.4 for SE-Short and 1.0 to 1.2 for SE-Long. This was be due to the design decision of adopting the least conservative displacement reduction factor (i.e., Eurocode 8-1994 [12]).

## 4. A proposed solution: the displacement-spectrum shape correction factor

The results discussed thus far show that the accuracy of the simplified method is greatly compromised in presence of simulated M9 CSZ motions. For the crustal and subduction zone earthquakes without basin effects, even though the median analysis-to-design ratios show a good match, the overall performance evaluated in terms of COV indicates that the accuracy of the design is also not ideal. However, it should be noted that the variability is partially due to the non-smoothness of the individual displacement spectra. To improve the accuracy of the simplified method, a displacement-spectrum shape correction factor, SCF, is proposed in this section.

The development of SCF was motivated by several factors as discussed here.

First, according to the equivalent lateral force procedure outlined in ASCE 7-16 [1], the maximum displacement of the isolation system (i.e. design displacement) should be calculated using:

$$D_M = \frac{gS_{M1}}{4\pi^2 B_M} T_M \tag{2}$$

where $g$ is the acceleration of gravity, $S_{M1}$ represents the $MCE_R$ 5% damped spectral acceleration parameter at 1-s period in units of g-sec, $T_M$ represents the effective natural period and $B_M$ is the numerical coefficients for the effective damping ratio of the isolation system at design displacement (i.e., inverse of the displacement reduction factor). This equation implies that the long-period branch of the displacement response spectrum is linear in period. Fig. 2a shows that the displacement spectra for Crustal motions are approximately linear with respect to period, whereas the displacement spectra for the simulated M9 motions are highly nonlinear with respect to period.

One of the key assumptions in the current design procedure is that the displacement reduction factor remains constant for a given damping ratio. To evaluate the accuracy of this assumption, the elastic displacement response spectrum at different damping ratios (10%, 20%, 30%, and 50%) were developed for all motions in all datasets. The obtained displacement spectra were then divided by the elastic displacement response spectrum at 5% damping ratio to calculate the displacement reduction factor for each ground motion.

Fig. 6 shows the comparison between the code displacement reduction factor from Eurocode 8-1994, and the average displacement reduction factor at different damping levels for each ground motion dataset. The average displacement reduction factor for the Crustal motion dataset between 1.5 and 5.0 s periods can be well approximated by a constant. This observation is consistent with the notion that the displacement reduction factor is period independent, as used in the code equations. The SE - short and SE - Long dataset also yield an approximately constant reduction factor, however the reduction is less than the equation used in Eurocode 8 (1994). This observation is consistent with the results that, when a more conservative displacement reduction equation was used, the accuracy of the results for SE - Short and SE - Long was improved [28]. For the M9 motion dataset, significant period dependency can be observed near periods of 1.0 s and 5.0 s.

Based on the above observations, a period-dependent displacement-spectrum shape factor is proposed as a measure of the level of "linearity" of the displacement spectrum.

### 4.1. Displacement-spectrum shape factor

To quantify the linearity of a displacement spectrum, a displacement-spectrum shape factor, $SS_d$, based on the elastic displacement spectrum at 5% damping is proposed and can be calculated as the area of region $A_1$ divided by the area of region $A_2$, which is shown in Fig. 7. It should be noted that this shape factor is unaffected by the scaling of the ground motion as both areas increase linearly with scale factors.

### 4.2. Displacement-spectrum shape correction factor

The correlation between the analysis-to-design ratios (Fig. 3) and their corresponding $SS_d$ values is shown in Eq. 3 and Fig. 8 for $\alpha$ equal to 3.0, corresponding to $T_2 = T_n$, and $T_1 = 0$. A line-of-best-fit is computed using regression analysis (using ordinary least squares) and found to have an $R^2$ of 0.55. Similar trends were found for all values of $\alpha$, where the $R^2$ value was found to be equal to 0.55, 0.55, 0.54, and 0.54 for $\alpha$ values of 2.0, 2.5, 3.5, and 4.0, respectively.

$$ln(\delta_{analysis}/\delta_{design}) = p1 \cdot SS_d + p2 \tag{3}$$

A critical input of the calculation of $SS_d$ is the period range of evaluating the linearity of the displacement spectrum. To examine this, a parametric study on the period range for calculating $SS_d$ was performed. The considered range of $T_1$ and $T_2$ were, respectively, from 0 to $0.8T_n$, and from $0.8T_n$ to $2T_n$. As shown in Fig. 9, the $R^2$ from linear regression analysis suggested that when $T_1$ equals 0 and $T_2 = T_n$, the correlation between the analysis-to-design displacement ratio and $SS_d$ can be best represented by a linear function. This implies that the linearity of displacement spectrum from 0 up to the equivalent natural period of the analyzed isolation system is significant to the accuracy of the simplified method.

### 4.3. Relationship between damping ratio and linear regression coefficients for spectral shape

The same analysis was performed considering all the other $\alpha$ values (from 2.0 to 4.0 with increments of 0.5). It was found that for different $\alpha$ values (i.e., damping ratios), the linear regression coefficients for the displacement-spectrum shape correction factor, SCF, are different. As shown in Fig. 10, the coefficients p1 and p2 vary linearly with $\alpha$ and they can be calculated using Eq. 4 and Eq. 5.

$$p1 = 0.27\alpha - 2 \tag{4}$$

$$p2 = -0.27\alpha + 2 \tag{5}$$

### 4.4. Correction factor and corrected results

Using Eqs. (3)–(5) above, the design-to-analysis displacement demand ratio can be related to the $SS_d$, and the resulting displacement-spectrum shape correction factor, SCF, can thus be calculated using Eq. 6:

$$\delta_{analysis} = \delta_{design} \cdot SCF = \delta_{design} \cdot [e^{-(0.27\alpha-2)(SS_d-1)}] \tag{6}$$

where $SS_d$ is calculated as illustrated in Fig. 7 using $T_1 = 0$ and $T_2 = T_n$. The corrected displacement demand can be obtained by multiplying the design displacement demand ($\delta_{design}$) by SCF. Fig. 11 shows how the design and analysis displacement demands are related without and with SCF applied for all periods and ground-motion sets. As expected, the correlation coefficient between the design and analysis displacement increased from 0.58 (Fig. 11a) to 0.75 (Fig. 11b) when applying SCF to

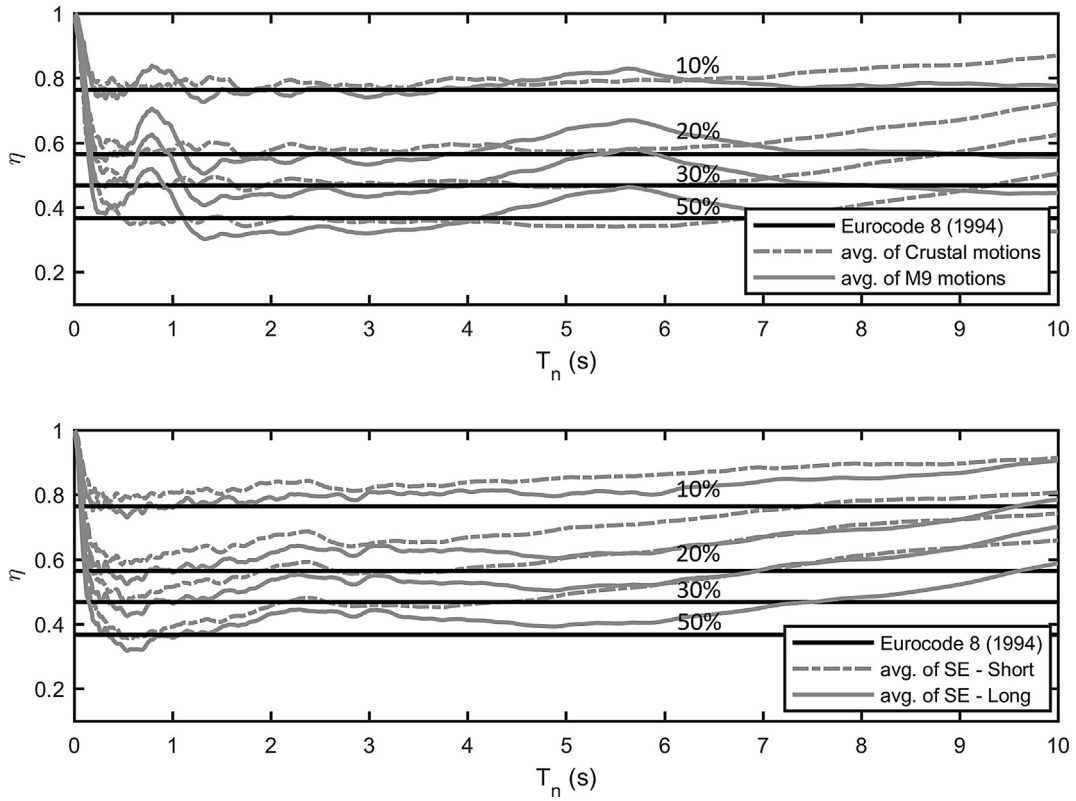


**Fig. 6.** Mean displacement reduction factors for (a) Crustal and M9 ground motions dataset and (b) SE - Short and SE - Long ground motion dataset. Mean displacement reduction factors predicted by Eurocode 8 (1994) [12] are also shown as black solid lines.

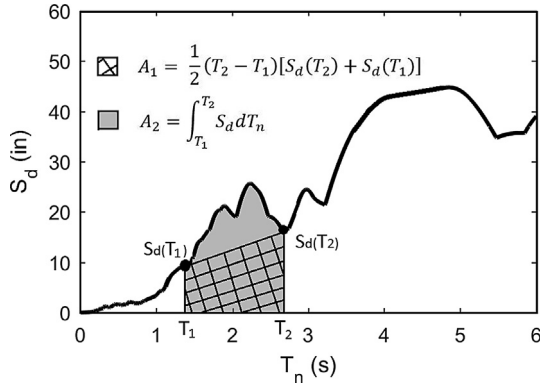


**Fig. 7.** Schematic illustration of calculating $SS_d$.

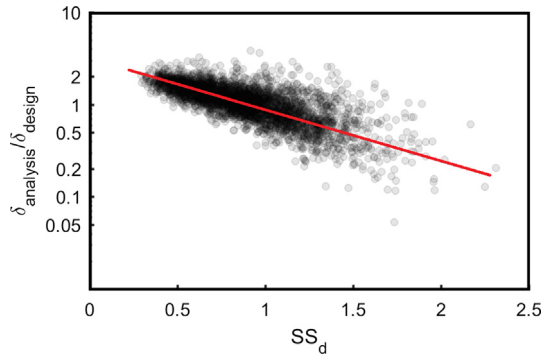


**Fig. 8.** Linear regression analysis between analysis-to-design displacement ratio and $SS_d$ for all data points in four ground motion datasets.

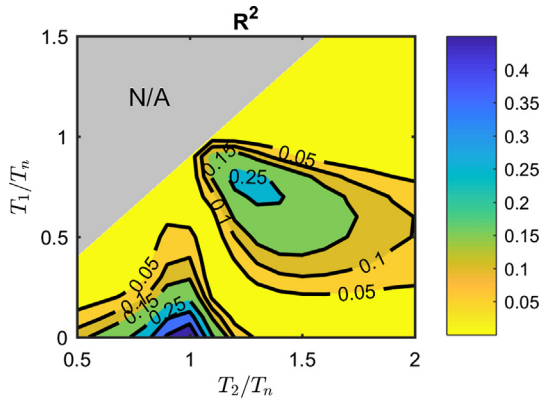


**Fig. 9.** $R^2$ for linear regression analysis varying the period range for calculating $SS_d$.

the design displacement. Table 1 shows the median and coefficient of variation values for each group motion dataset with and without SCF.

Fig. 12 shows the comparison of analysis-to-design ratios with and without the SCF applied with respect to period for each ground-motion set. It can be observed that after applying SCF, the median ratios of all groups are approximately one (summarized in Table 1). The overall variability in the analysis-to-design ratio was significantly improved as quantified using the coefficient of variation. Fig. 13 shows the comparison of COV of analysis-to-design ratios with and without the SCF applied with respect to period for each ground-motion set. Fig. 13 and Table 1 show that the COV reduced by approximately 20% in all ground motion sets. It is worth mentioning that the COV of the analysis-to-design ratio for M9 motion dataset increased at periods 1.5 s and 2.0 s. While the reasons for this increase remain unclear, it should be noted that FPS isolated systems typically have equivalent natural period values above 2.0 s. Thus this increase in COV at low periods does not

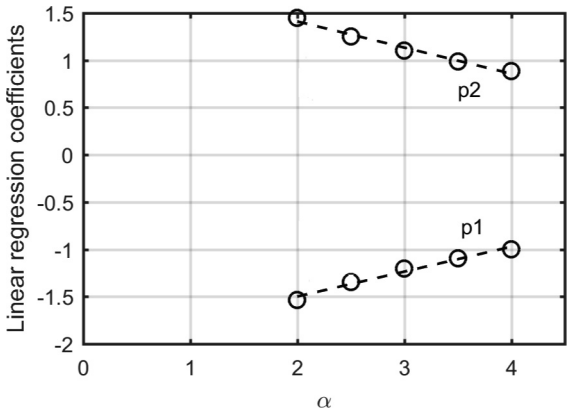


**Fig. 10.** Relationship between $\alpha$ and the linear regression coefficients in displacement-spectrum shape correction factor.

affect practical design of FPS isolated systems.

The same numerical analyses procedure were also performed using the displacement reduction equation/table provided by Eurocode 8 (2004) [2], and ASCE 7-16 [1]. As mentioned, only the final outcome is shown in this paper, detailed results can be found in Yang [28]. The calibrated SCFs are shown in Eq. 7 and Eq. 8. They yielded similar extent of improvement as those outlined in previous sections, pertaining to systems designed using the displacement reduction equation provided by Eurocode 8 (1994) [12].

$$SCF_{EC8-2004} = e^{-(0.33\alpha-2.44)SS_d+0.30\alpha-2.02} \quad (7)$$

$$SCF_{ASCE7-16} = e^{-(0.41\alpha-2.82)SS_d+0.32\alpha-2.07} \quad (8)$$

It should be noted that the presented SCF can also be implemented into the iterative procedure outlined in Section 2. One could use SCF at the end of each iteration to correct the displacement demand. This corrected value can then be compared with the displacement demand value from the previous iteration. The final displacement demand is determined when it converges to the previous iteration.

## 5. Conclusions

This paper evaluated the accuracy of the simplified design method for seismic isolation systems that is the basis for many international code provisions in the context of Friction Pendulum Systems subjected to subduction zone and basin amplified ground motions. The results showed that the simplified method predicts the maximum displacement observed from analysis with insufficient accuracy, producing estimates of peak displacement that are reasonable on-average but with significant scatter. A new correction parameter (i.e. displacement-spectrum shape correction factor) was introduced that improved the accuracy of the simplified design method.

In the current simplified design method, the displacement demand is estimated by linearizing the isolation system characterized by the effective stiffness and the effective damping ratio at the design displacement. The accuracy of this method was evaluated using non-linear time history analyses of FPS with equivalent natural periods ranging from 1.5 to 5.0 s and equivalent damping ratios ranging from 16% to 32%. These analyses were run for four sets of ground motions from (1) Crustal earthquakes, (2) simulated magnitude-9 earthquakes from the Cascadia Subduction Zone which include deep sedimentary basin effects, (3 & 4) and spectrally equivalent pairs from crustal and subduction zones. Three displacement reduction equations/table were considered in this study: (1) Eurocode 8 (1994), which is the same equation recommended by Priestley et al. [13], (2) Eurocode 8 (2004), and (3) ASCE 7-16. For each of the nonlinear time-history analysis, the ratio between the peak displacement recorded from the analysis and the design displacement was computed. The following conclusions can be drawn from the results of this study:

- For all three considered displacement reduction equations, the simplified method provided good approximations of the median of the maximum displacement when Crustal motion dataset and spectrally equivalent (SE - Long and SE - Short) dataset were used. Of the three displacement reduction equations, for Crustal motion dataset, Eurocode 8 (1994) provided the most accurate results, with a median analysis-to-design ratio of approximately 1.0 for all the equivalent natural periods and damping ratios considered. Eurocode 8 (2004) and ASCE 7-16 yielded conservative results, with median analysis-to-design ratios of 0.85 and 0.78, respectively. For spectrally equivalent dataset, Eurocode 8 (2004) provided the most accurate results, with a median analysis-to-design ratio of approximately 1.0. Eurocude 8 (1994) and ASCE 7-16 had median analysis-to-design ratios of 1.2 and 0.9, respectively.
- The median maximum displacement values from the analyses did not match the design displacement values from nonlinear analysis for the M9 motion dataset for all considered displacement reduction equations/table. For lower equivalent natural periods, the design was overly conservative. In contrast, the simplified method provided unconservative displacement demands at long periods (i.e. 4.5 s and above).
- For all datasets, the overall performance of the simplified method was not sufficient because of the large observed variance in the analysis-to-design ratios (coefficient of variation ranged from 13%

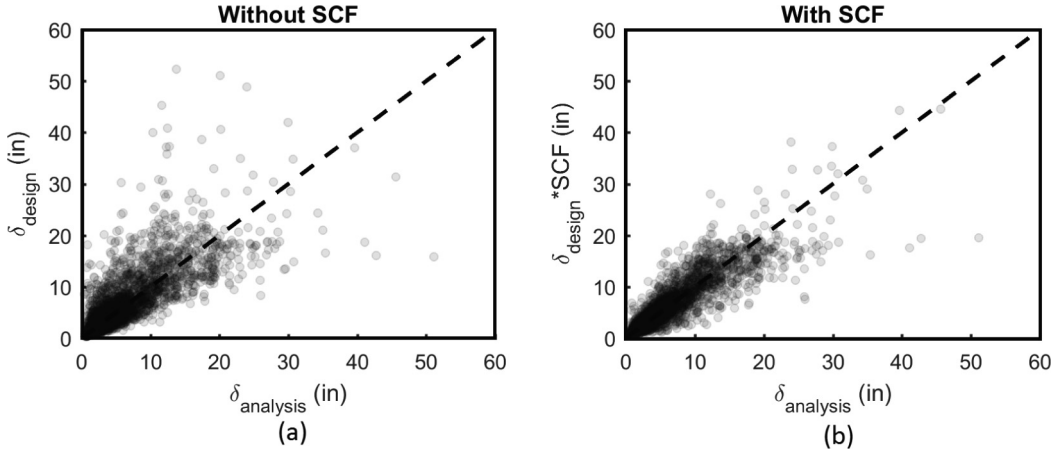


**Fig. 11.** Comparison of maximum absolute displacement from analysis and design displacement for all periods and ground-motion sets (Crustal, M9, SE - Short, SE - Long) (a) without applying SCF and (b) with applying SCF.

**Table 1**
Median and coefficient of variance comparison before and after applying SCF for each ground motion dataset.

| GM | Crustal | | M9 | | SE-Short | | SE-Long | |
|---|---|---|---|---|---|---|---|---|
| | w/o SCF | w/SCF | w/o SCF | w/SCF | w/o SCF | w/SCF | w/o SCF | w/SCF |
| 50*thper*. | 0.93 | 1.01 | 0.81 | 0.90 | 1.26 | 1.04 | 1.13 | 0.97 |
| COV | 0.13 | 0.10 | 0.24 | 0.19 | 0.23 | 0.16 | 0.23 | 0.18 |

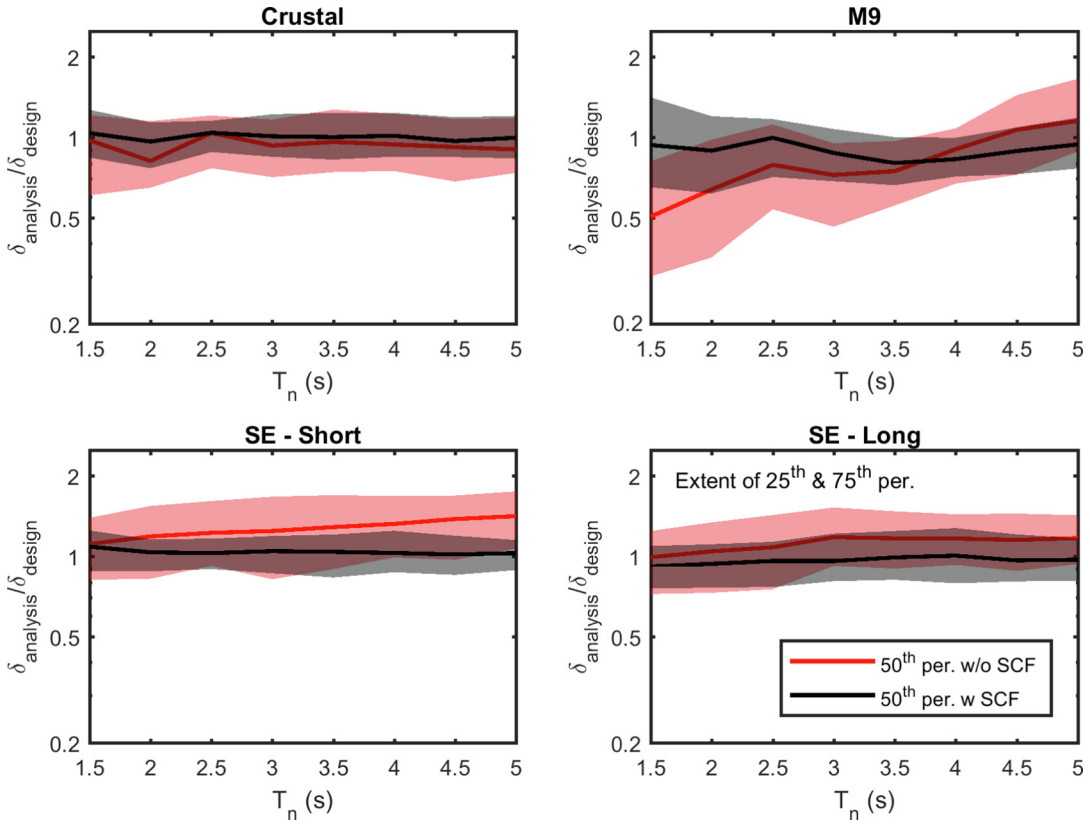


**Fig. 12.** Boxplot comparison before and after applying displacement-spectrum shape correction factor, varying by equivalent natural period and ground motion dataset.

to 24%).

To improve the accuracy of the simplified method, a displacement-spectrum shape correction factor was introduced. This shape correction factor takes into account the nonlinearity of the elastic displacement spectrum at 5% damping ratio, and the effective period and effective damping ratio of the FPS at design displacement. The displacement-spectrum shape correction factor was calibrated for all three considered design provisions. Applying the shape correction factor resulted in analysis-to-design ratios median of 0.99 (from 1.1) and a coefficient of variation of 16% (from 24%), for all considered ground motion datasets.

While the results of this study are intended for use with FPS isolated structures, they may be applicable to other systems characterized by bi-linear hysteresis such as lead-rubber bearings. However, until this is verified as part of future research, the conclusions presented in this paper should be limited to Friction Pendulum Systems.

It should be noted that the modelling methodology for the friction coefficient used in this study does not consider the effect of velocity, pressure, cyclic degradation or temperature [30–32]. Future work shall consider the effectiveness of the proposed shape correction factor in NLTHA with models that account for these effects.

## CRediT authorship contribution statement

**Tianye Yang:** Conceptualization, Methodology, Software, Formal analysis, Writing - original draft. **Nasser A. Marafi:** Methodology, Data curation, Writing - review & editing. **Paolo M. Calvi:** Methodology, Supervision, Writing - review & editing. **Richard Wiebe:** Methodology, Supervision, Writing - review & editing. **Marc O. Eberhard:** Methodology, Supervision, Writing - review & editing. **Jeffrey W. Berman:** Methodology, Supervision, Writing - review & editing.

## Declaration of Competing Interest

The authors declare that they have no known competing financial interests or personal relationships that could have appeared to influence the work reported in this paper.

## Acknowledgment

This research was funded by the National Science Foundation under Grant No. EAR-1331412. The authors would like to thank (1) Arthur Frankel and Erin Wirth for sharing the results of their simulations of M9 CSZ interface earthquakes, (2) Reagan Chandramohan for sharing the spectrally matched short and long duration set. Any opinion, findings,

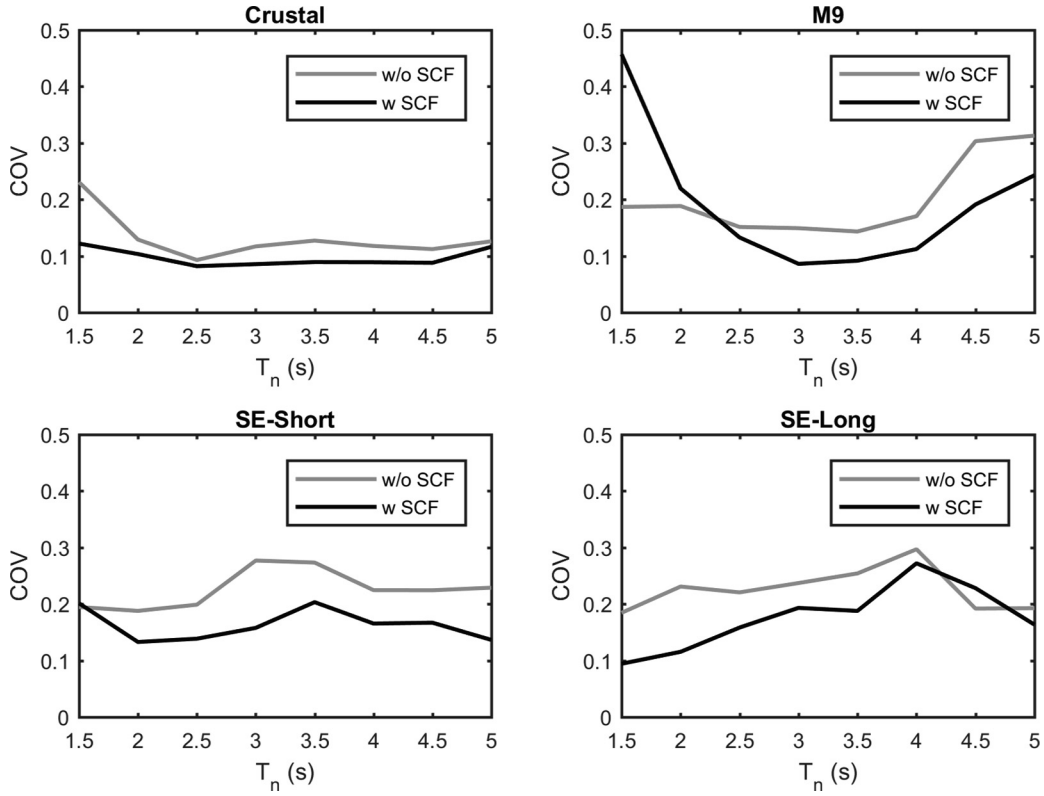


**Fig. 13.** Coefficient of variance (COV) comparison before and after applying displacement spectrum shape correction factor, varying by equivalent natural period and ground motion dataset.

and conclusions or recommendations expressed in this material are those of the authors and do not necessarily reflect the views of the collaborators or sponsoring agencies.

## References


[1] ASCE. Asce/sei 7-16: Minimum design loads and associated criteria for buildings and other structures; 2017.
[2] EC8. En 1998-1 eurocode 8: Design of structures for earthquake resistance - part 1: General rules, seismic actions and rules for buildings; 2004.
[3] Kircher CA, Lashkari B. Statistical evaluation of nonlinear response of seismic isolation systems. Tech. Rep. JBA 109-070. Mountain View, USA, CA: Jack R. Benjamin and Associates, Inc.; 1989.
[4] Winters CW, Constantinou MC. Evaluation of static and response spectrum analysis procedures of seaoc/ubc for seismic isolated structures. Tech. Rep. NCEER 93-0004. Buffalo, NY, USA: National Center for Earthquake Engineering Research, University at Buffalo, State University of New York; 1993.
[5] Tsopelas P, Constantinou MC, Kircher CA, Whitaker AS. Evaluation of simplified methods of analysis for yielding structures. Tech. Rep. NCEER 97-0012. Buffalo, NY, USA: National Center for Earthquake Engineering Research, University at Buffalo, State University of New York; 1997.
[6] Miranda E, Ruiz-Garcia J. Evaluation of approximate methods to estimate maximum inelastic displacement demands. Earthquake Eng Struct Dynam 2002;31(3):539–60.
[7] Guyader AC, Iwan WD. Determining equivalent linear parameters for use in a capacity spectrum method of analysis. J Struct Eng (ASCE) 2006;132(1):59–67.
[8] Pavlou EA, Constantinou MC. Response of elastic and inelastic structures with damping systems to near-field and soft-soil ground motions. Eng Struct 2004;26(9):1217–30.
[9] Graves RW, Pitarka A, Somerville PG. Ground-motion amplification in the santa monica area: Effects of shallow basin-edge structure. Bull Seismol Soc Am 1998;88(5):1224–42.
[10] Frankel A, Stephenson W, Carver D. Sedimentary basin effects in Seattle Washington: ground-motion observations and 3d simulations. Bull Seismol Soc Am 2009;99(3):1579–611.
[11] Marafi NA, Eberhard MO, Berman JW, Wirth EA, Frankel A. Effects of deep basins on structural collapse during large subduction earthquakes. Earthquake Spectra 2017;33(3):963–97.
[12] EC8. nv 1998-1-2 eurocode 8: Design provisions for earthquake resistance of structures - part 1-2: General rules - general rules for buildings.
[13] Priestley MJN, Calvi GM, Kowalsky MJ. Displacement based seismic design of structures. Pavia, Italy: IUSS Press; 2007.
[14] Lin YY, Chang KC. Study on damping reduction factor for buildings under earthquake ground motions. J Struct Eng 2003;129(2):206–14.
[15] Bommer Jj, Mendis R. Scaling of spectral displacement ordinates with damping ratios. Earthquake Eng Struct Dyn 2005;34(2):145–65.
[16] Lin YY, Chang KC. Effects of site classes on damping reduction factors. J Struct Eng 2004;130(11):1667–75.
[17] PEER. Pacific earthquake engineering research center, next generation attenuation (nga) - west2; 2010. URL https://peer.berkeley.edu/research/nga-west-2.
[18] NEHRP. Nehrp recommended seismic provisions for new buildings and other structures; 2015 edition.
[19] Atwater B, Nelson A, Clague J, Carver GA, Yamaguchi DK, Bobrowsky PT, et al. Summary of coastal geologic evidence for past great earthquakes at the cascadia subduction zone. Earthquake Spectra 1995;11(1):1–18.
[20] Goldfinger C, Nelson CH, Morey AE, Johnson JE, Patton JR, Karabanov EB, et al. Turbidite event history - methods and implications for holocene paleoseismicity of the cascadia subduction zone. Report 1661. Reston, VA, USA: U.S. Geological Survey; 2012.
[21] Stephenson WJ, Reitman NG, Angster SJ. P- and s-wave velocity models incorporating the cascadia subduction zone for 3d earthquake ground motion simulations, Report 2017–1152. Reston, VA, USA: U.S. Geological Survey; 2017.
[22] Frankel A, Wirth EA, Marafi NA, Vidale J, Stephenson WJ. Broadband synthetic seismograms for magnitude 9 earthquakes on the cascadia megathrust based on a 3d simulation and stochastic synthetics, part 1: methodology and overall results. Bull Seismol Soc Am 2018;108(5A):2347–69.
[23] Chandramohan R, Baker JW, Deierlein GG. Quantifying the influence of ground motion duration on structural collapse capacity using spectrally equivalent records. Earthquake Spectra 2016;32(2):927–50.
[24] PEER. verson 2.5.0. Berkeley, CA, USA: Pacific Earthquake Engineering Research Center, University of California; 2006.
[25] Mosqueda G, Whittaker AS, Fenves GL. Characterization and modeling of friction pendulum bearings subjected to multiple components of excitation. J Struct Eng 2004;130(3):433–42.
[26] Calvi PM, Moratti M, Calvi GM. Seismic isolation devices based on sliding between surfaces with variable friction coefficient. Earthquake Spectra 2016;32(4):2291–315.
[27] Calvi PM, Calvi GM. Historical development of friction-based seismic isolation systems. Soil Dyn Earthquake Eng 2018;106:14–30.
[28] Yang T. High performance friction-type bearings for seismic isolation. Ph.D. thesis; 2020.
[29] Marafi NA, Eberhard MO, Berman JW, Wirth EA, Frankel A. Impacts of m9 cascadia subduction zone earthquake on idealized systems. Earthquake Spectra 2019;35(3):1261–87.
[30] Kumar M, Whittaker AS, Constantinou MC. Characterizing friction in sliding isolation bearings. Earthquake Eng Struct Dynam 2014;44(9):1409–25.
[31] Lomiento G, Bonessio N, Benzoni G. Friction model for sliding bearings under seismic excitation. J Earthquake Eng 2013;17(8):1162–91.
[32] Gandelli E, Penati M, Quaglini V, Lomiento G, Miglio E, Benzoni G. A novel opensees element for single curved surface sliding isolators. Soil Dyn Earthquake Eng 2019;119:433–53.